Fabrizio Nestola

5 Ringwoodite: its importance in Earth Sciences

5.1 History of ringwoodite

The history of ringwoodite started in 1869 in a remote locality in the south-west of Queensland in Australia. Mr. Michael Hammond witnessed a meteorite shower close to the junction between Cooper and Kyabra Creeks (Lat. 25° 30′ S., Long. 142° 40′ E.), not far from Windorah (Queensland, Australia) and about 1000 km west of Brisbane. The meteorite fall was very impressive and in due course 102 stones were recovered. Mr. Hammond was the owner of the Tenham Station and from this the meteorite collection was named as "Tenham meteorites". This collection was then offered in 1935 to the British Museum by Mr. Benjamin Dunstan, formerly Government Geologist of Queensland [1].

But why does this nice story match with ringwoodite? In 1969, exactly 100 years after Mr. Hammond observed the Tenham meteorite fall, R. A. Binns, R. J. Davies and S. J. B. Reed published in Nature [2] the first natural evidence of ringwoodite after studying a fragment of the Tenham meteorite. Thirty years later Chen et al. [3] reported clear images of some lamellae of about 1–2 μ in thickness showing a higher density than olivine but with identical composition (Fig. 5.1, modified from Chen et al. [3]). The
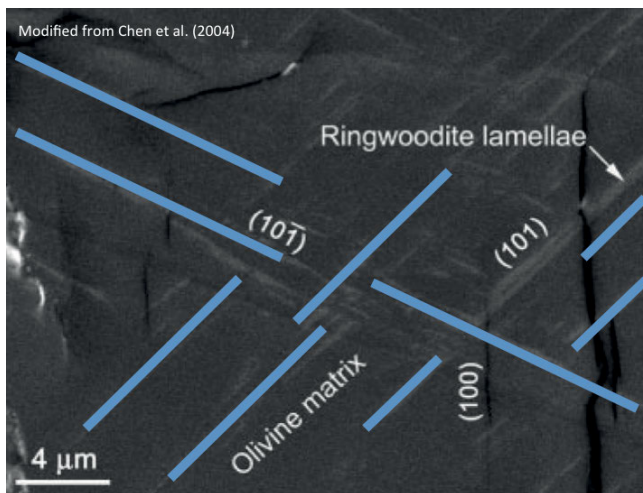

Fig. 5.1: Back-scattered image of lamellae of ringwoodite in olivine (modified from [3]). The lamellae are evident being marked by a brighter grey. The darker grey corresponds to olivine. The blue solid lines are reported to indicate the directions along which ringwoodite grew. In white parentheses the lattice planes are indicated. The thickness of the lamellae could be on the sub-μm scale.

X-ray powder diffraction data of the same lamellae inside olivine [2] indicated cubic symmetry with the cell edge $a = 8.113(3)$ Å. This discovery showed that this new cubic polymorph of olivine was identical to the phase synthesized three years earlier [4] at about 17 GPa and a temperature estimated to be around 900 °C. This cubic polymorph was obtained at experimental conditions typical of deep mantle, demonstrating that this phase could be a major component of this layer of our planet. Thus, a proposal for a new mineral was submitted [2] to the International Mineralogical Association (IMA) leading to approval of this new cubic polymorph of olivine as RINGWOODITE (IMA 1969-038). The name was given in honor of Prof. Alfred Edward Ringwood of the Australian National University for his experimental studies on petrology, phase transformations, constitution, and dynamics of the mantle.

The stability field of ringwoodite falls within the *P-T* conditions of the so-called transition zone. The transition zone extends between 410 and 660 km depth. It does not show any complex thermal or chemical structure and is not subject to melting processes, which usually occur in the shallower region of the upper mantle [5]. According to Frost [6] the transition zone is characterized by some seismic discontinuities [7, 8] that should be related to mineral phase transformations. The phase assemblage of the transition zone mainly consists of ringwoodite, wadsleyite and majoritic garnet. Fig. 5.2 is a representation of the mineral volume-fraction in this layer (modified
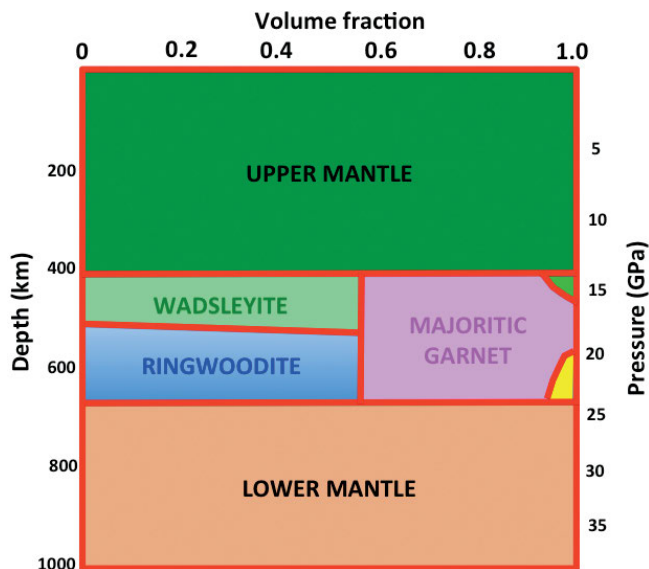

Fig. 5.2: Volume fraction of the transition zone between 410 and 660 km showing the three main phases ringwoodite, wadsleyite and, majoritic garnet (modified from [5]). In addition to the main phases diopside (light green) and in yellow $CaSiO_3$ (likely with walstromite-like structure) are displayed. Above and below the transition zone the upper mantle (dark green) and the lower mantle (light orange) are shown.

from Frost [5]). The diagram shows that the transition zone is constituted of about 41 % majoritic garnet, about 34 % ringwoodite, 23 % wadsleyite and the remaining 2 % are $CaSiO_3$ and $CaMgSi_2O_6$ diopside. In Fig. 5.2 the green area represents about 60 % olivine, which transforms to wadsleyite at a depth of about 410 km, which in turn transforms to ringwoodite at about 525 km [5]. Finally, ringwoodite breaks down to ferropericlase (Mg,Fe)O plus bridgmanite $MgSiO_3$ (perovskite-type structure). The reader is referred to chapter 4 for a more detailed discussion on structure and sharpness of the transition zone and thus the actual extension of the ringwoodite stability field.

5.2 Crystal structure and Mg/Fe substitution

For a better distinction from its lower-pressure polymorphs wadsleyite and common olivine, ringwoodite is also known as γ-olivine. Wadsleyite and olivine are called [9] β-olivine and α-olivine, with *Imma* and *Pbnm* symmetry (both orthorhombic), respectively. Thus, the two former modifications are symmetrically distinct from cubic γ-olivine of the $Fd\bar{3}m$ space group. Hereafter we will use the IMA mineral name ringwoodite, olivine (group name), and wadsleyite.

Ringwoodite has the chemical formula $(Mg,Fe)_2SiO_4$. The Fe dominant member was recently discovered in the Martian meteorite Tissint and named ahrensite ([10], IMA 2013-028, in honor of T.J. Ahrens (1936–2010), geophysicist at California Institute of Technology).

The ringwoodite-ahrensite solid solution shows complete miscibility as demonstrated by synthetic samples, e.g. [11–13]. Optical and physical properties for the two end-members are reported in Tab. 5.1. Ringwoodite and ahrensite crystallize in the spinel structure-type with space group $Fd\bar{3}m$. For comparison, the crystal structures of ringwoodite, olivine and wadsleyite are shown in Fig. 5.3.

Tab. 5.1: Physical and optical properties for ringwoodite and ahrensite.

	Ringwoodite	Ahrensite
Refractive index *n*	1.768	1.895*
Relief	High	High
Colour	Blue, deep blue, purple	Black
Calculated density	3.56 g/cm^3	4.98 g/cm^3
Hardness (Mohs)	7–7.5	

* estimated from the density differences between forsterite-fayalite and ringwoodite-ahrensite

Ringwoodite and olivine group minerals are both classified as orthosilicates. In these minerals, SiO_4 tetrahedra are isolated and not connected to other tetrahedra. In contrast, the crystal structure of wadsleyite has one oxygen (O2) connecting two tetrahe-
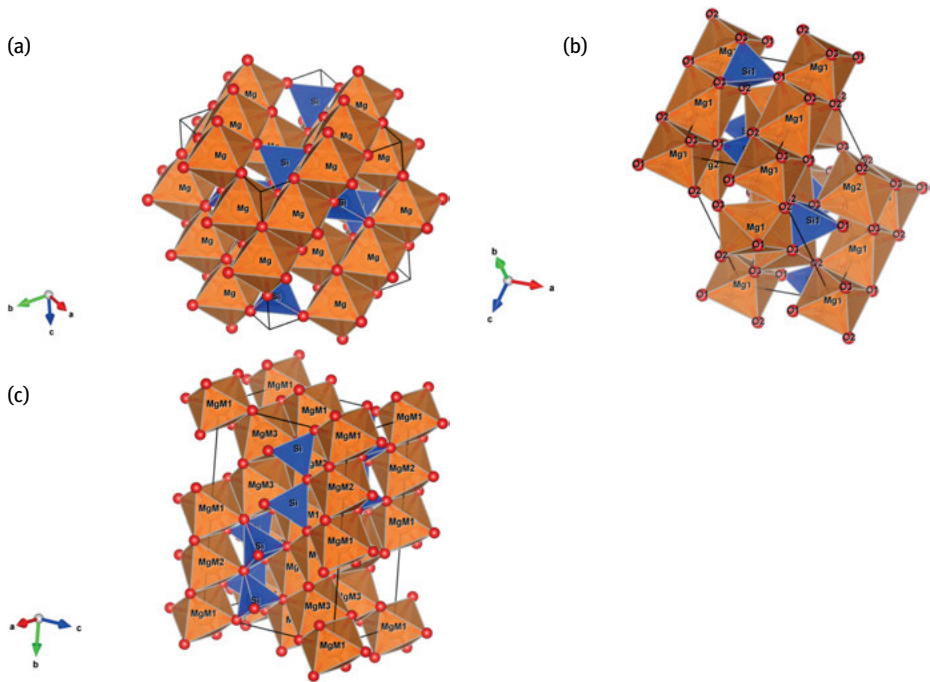
(a)

(b)

(c)

Fig. 5.3: Crystal structure of ringwoodite (a), forsterite (b) and wadsleyite (c). The structural data were from [11], [15] and [16], respectively. The orange octahedra are always relative to Mg, whereas the deep violet tetrahedra refer to Si. The red spheres correspond to oxygen atoms. The thin solid lines show the unit cell for each polymorph. The structures were drawn using Vesta software.

dra forming an Si_2O_7 group and is classified as sorosilicate. Ringwoodite has only one regular octahedron (with all Mg-O distances having the same length). Olivine has two (M1 and M2) more irregular octahedra, and wadsleyite has three symmetry independent M1, M2, and M3 octahedra (see Fig. 5.3).

Already in 1968 Kamb [14] explained on a structural basis, the reason why ringwoodite is the stable Mg_2SiO_4 form at high pressure. In case of olivine, wadsleyite, and ringwoodite the transformations are not driven by changes in the cation coordination number as observed for several other silicates. The olivine structure is based upon a non-ideal hexagonal-closest packed arrangement of oxygen atoms, with Si in tetrahedral coordination and Mg/Fe in octahedral coordination. In contrast, ringwoodite shows a cubic-closest packed arrangement of O atoms with Si and Mg/Fe having the same coordination number as in olivine. In general terms, this arrangement in olivine and ringwoodite should at first glance yield similar densities. This, however, is not the case. Actually, the density of ringwoodite is about 10 % higher than that of forsterite (olivine). We know that the higher density is the main reason for the stabilization of a polymorph to higher pressure, therefore, it is important to understand

the structural reason for the higher density of end-member ringwoodite compared to end-member forsterite. The major reason for the density difference is the cation distribution in the second coordination sphere, considering also metal-metal (Si,Mg) distances [15]. The spinel structure exhibits six shared edges among adjacent octahedra whereas the olivine structure has on average (M1, M2) three shared octahedral edges and additionally three shared edges between MgO_6 octahedra and SiO_4 tetrahedra.

Only part of the density difference can be attributed to the average Mg-O distance, which is longer in olivine (about 2.120 Å, [15]) and significantly shorter in ringwoodite (2.066 Å, [11]). According to Kamb [14] the cause can be attributed to the shortening of shared polyhedral edges. The c axis in olivine is twice the Mg1-Mg1 distance (2.99 Å) across the shared octahedral edges whereas along the corresponding direction in ringwoodite the distance is only 2.85 Å contributing with a factor of 1.049 to the increased density (2.99 Å$_{olivine}$/$2.85_{ringwoodite}$ Å = 1.049). The length of the a axis in olivine is affected by the distortion of the SiO_4 tetrahedron. In particular, the distance from base to vertex of the tetrahedron in olivine is about 2.85 Å and only 2.7 Å in ringwoodite. Such a difference of 0.15 Å contributes to an elongation of the a axis in olivine by a factor of 1.033 (doubled distances: 4.70 Å$_{olivine}$/$4.55_{ringwoodite}$ Å = 1.033). If these two factors are combined with the difference in the average Mg-O distance (i.e. 2.12 Å$_{olivine}$/$2.066_{ringwoodite}$ Å = 1.027), an increased density $d = 3.59$ g/cm^3 is estimated for ringwoodite relatively to the density of 3.23 g/cm^3 for forsterite. This simple calculation matches the experimental density of Mg ringwoodite.

The above reasoning can also be applied to the intermediate-pressure polymorph wadsleyite ($d = 3.47$ g/cm^3). Wadsleyite is considered a spinelloid and as such also based on a distorted cubic closest packing of O. M1 and M2 octahedra have six shared edges while M3 has seven. The average Mg-O distance in wadsleyite is 2.082 Å [16] while Mg-O in ringwoodite is 2.066 Å. This difference contributes to an increase of ringwoodite density by only 1 % (i.e. 2.082 Å$_{wadsleyite}$/$2.066_{ringwoodite}$ Å = 1.01). Along the b axis wadsleyite has a distance between Mg1 and Mg2 equal to 2.870 Å, which is slightly longer than that of ringwoodite along a corresponding direction. This difference only justifies a density increase by about 0.7 % (2.870 Å$_{wadsleyite}$/$2.850_{ringwoodite}$ Å = 1.007). However, along a direction close to [111] in wadsleyite the distance Mg1–Mg3 is 2.902 Å, while in ringwoodite the corresponding distance is only 2.850 Å (2.902 Å$_{olivine}$/$2.850_{ringwoodite}$ Å = 1.018). Thus, starting from the density of wadsleyite $d = 3.47$ g/cm^3, multiplied by 1.010 ×1.007 ×1.018 leads to $d = 3.59$ g/cm^3 for ringwoodite, again a perfect match with observation.

The structural parameters of ringwoodite and ahrensite are reported in Tab. 5.2. The available data on ringwoodite-ahrensite were collected [17] on synthetic samples as no natural crystals suitable for structural investigation have been found so far. This could be important to better understand whether in the Earth mantle the octahedral site in ringwoodite and ahrensite can be partly occupied by Si replacing Mg/Fe. Si in octahedral coordination, indeed, is a remarkable feature of some high-pressure minerals like majoritic garnet (i.e. [18, 19]) and stishovite (the high-pressure poly-

Tab. 5.2: Crystal-structure parameters for ringwoodite (Mg_2SiO_4) and ahrensite (Fe_2SiO_4).

Mineral	Cell edge a (Å)	Oxygen coordinate u ($x = y = z$)	Si coordinate ($x = y = z$)	Mg coordinate ($x = y = z$)	Si – O (Å)	V_{SiO4} (Å^3)	Mg–O (Å)	V_{MgO6} (Å^3)
Ringwoodite	8.0709(2)	0.2441(1)	0.125	0.5	1.6650(5)	2.369(2)	2.0664(3)	11.727(5)
				Fe coordinate ($x = y = z$)			Fe – O (Å)	V_{FeO6} (Å^3)
Ahrensite	8.2312(2)	0.2420(4)	0.125	0.5	1.668(6)	2.382(10)	2.125(4)	12.732(34)

Notes: ringwoodite data were taken from [11], whereas the data for synthetic ahrensite are from [17]

morph of silica has Si only in octahedral coordination with average Si-O distance being 1.775 Å, see [20]). In particular, the case of majoritic garnet is of special importance as this phase is thought to be the most abundant phase of the transition zone: a typical natural majoritic garnet with respect to the ideal synthetic end-member, Mg_3 ^{VI}(MgSi)Si_3O_{12}, shows in the octahedral ^{VI}(MgSi) site about 0.3–0.4 Si atoms per formula unit (apfu) based on 12 O, Al close to 0.9–1.0 apfu, Fe^{2+} close to 0.5 apfu and some Ti^{4+} [19] However, Nakatsuka and coauthors [18] studying the structural change along the synthetic join $MgSiO_3 - Mg_3Al_2Si_3O_{12}$ found that for Si between 0.24 and 0.38 apfu the typical garnet symmetry $Ia\bar{3}d$ changes to tetragonal $I4_1/acd$. This was confirmed by diffraction data and supported by optical evidence. Independent of symmetry, in majoritic garnets Si occurs in both tetrahedral and octahedral coordination.

Ringwoodite synthetized at 20 GPa and 1400 °C may contain about 4 % of Si_{tot} at the octahedral site [21]. The presence of six-coordinated Si could be favored by high temperature [12] under these mantle-like pressure conditions. Surprisingly, for the Fe-richer samples Si does not show any tendency [11] to enter the octahedral site. It has not yet been investigated whether Si/Mg disorder is a peculiar characteristic of synthetic samples or whether it is also typical of natural samples. Hazen and coauthors [11] propose for their synthetic Mg end-member ringwoodite the crystal chemical formula ($Mg_{1.96}Si_{0.04}$)($Si_{0.96}Mg_{0.04}$)O_4 and infer a double substitution $^{VI}Mg^{2+} + {}^{VI}Si^{4+} = {}^{IV}Mg^{2+} + {}^{IV}Si^{4+}$ to maintain charge balance.

5.3 The effect of water on the crystal structure of ringwoodite

In 1987 Smyth [22] suggested that hypothetically wadsleyite, the polymorph stable in the transition zone together with ringwoodite and majoritic garnet, could host a considerable amount of water and therefore possibly act as a significant mantle water reservoir. Although, there was actually no evidence of water (in terms of OH groups) in wadsleyite, Smyth [22] claimed that if this could be demonstrated then it could have substantial consequences for geophysical and geochemical models of the upper mantle. Just some years later, up to 3.1 wt.% H_2O in wadsleyite were experimentally demonstrated [9, 22, 23], confirming the hypothesis [22] about the capacity of

such phases to host substantial amounts of water. At the same time, experimental evidence [9] demonstrated water solubility up to 2.7 wt.% H_2O in terms of OH groups in ringwoodite.

In the decade from 1985–1995 several experimental studies dealing with the synthesis of dense Mg-silicates focused on water storage under mantle conditions [24]. However, among all hydrous Mg-silicates only wadsleyite and ringwoodite could have a significant impact on the mantle geophysics and geochemistry and thus most projects focused on these two phases.

In the first study dealing with the influence of water on the ringwoodite structure, Smyth and coauthors [25] investigated seven samples of hydrous ringwoodite with compositions between Fo_{100} and Fo_{89} and H_2O contents between 0.2 and 1.1 wt.% [a typical composition of their sample was $Mg_{1.633}Fe^{2+}_{0.231}Fe^{3+}_{0.026}Si_{0.999}(H_{0.174})O_4$]. The samples, synthesized from 18 to 22 GPa and 1400 to 1500 °C, were analyzed by single-crystal X-ray diffraction, Fourier-transform infrared (FTIR) spectroscopy, Mössbauer spectroscopy, wave length dispersive spectroscopy (WDS) using an electron microprobe, and transmission electron-microscopy (TEM). It could be shown [26] that the principal hydration mechanism involves octahedral cation vacancies with the occupancy of the octahedral site appearing to decrease systematically with H content.

Results of Mössbauer studies indicated that Fe^{3+} is negligible (i.e. maximum content 0.026 apfu) and thus does not affect the crystal structure. The influence of Fe^{2+} on the structure of ringwoodite has already been discussed in the previous section. Let us consider the H-richest ringwoodite sample [25] SZ0104 with the chemical formula $Mg_{1.633}Fe^{2+}_{0.231}Fe^{3+}_{0.026}Si_{0.999}(H_{0.174})O_4$, which contains about 1.1 wt.% H_2O.

For anhydrous ringwoodite, complete replacement of Mg by Fe^{2+} (i.e. ahrensite end-member) causes an increase of the octahedral M-O (M = Mg/Fe) bond lengths by about 0.0006(3) Å/(0.01 molar fraction). Therefore, an increase in M-O = 2.0736 Å should be expected due to the Fe content in SZ0104, which is 0.129 in molar fraction. Instead the M-O bond length for hydrous ringwoodite SZ0104 is considerably longer with M-O = 2.0809(6) Å. The same logic applies to the unit-cell volume, which for a ringwoodite with starting composition $Mg_{1.742}Fe_{0.248}$, like SZ0104, should be 529.85(10) Å^3; instead the observed volume is 532.49(7) Å^3. Thus, in ringwoodite containing 1.1 wt.% H_2O the M-O distance is increased by 0.007 Å and the unit-cell volume by 2.6 Å^3.

More recently [24], Fe-free hydrous ringwoodite hosting 2.5 wt.% H_2O (measured by secondary ion mass spectroscopy) revealed a similar effect of H_2O on its crystal structure: the Mg-O distance increased by 0.006 Å and the unit-cell volume by 2.09 Å^3, relative to the prediction for the anhydrous composition. Panero et al. [26], studying similar samples at different pressure and temperature conditions, found different substitution mechanisms for OH groups in the ringwoodite structure. Both the Mg octahedra and Si tetrahedra may host H by a typical hydrogarnet substitution [26]. An increase in the unit-cell volume of 2.09 Å^3 due to 2.5 wt.% H_2O in ringwoodite corresponds to an expansion caused by a temperature increase of 140 °C.

5.4 Ringwoodite stability field

The Mg_2SiO_4-Fe_2SiO_4 system was studied at 1400 °C as a function of pressure and Fe/(Fe+Mg) ratio [6]. For the Mg end-member olivine transforms to wadsleyite slightly above 14 GPa and wadsleyite transforms to ringwoodite at about 20 GPa (Fig. 5.4). With increasing Fe the average transformation pressure decreases and at the same time the transformations occur within a significantly broader pressure interval. In general, it is observed (Fig. 5.4) that at 1400 °C the minimum pressure at which ringwoodite can exist reduces from 20 GPa for the pure Mg end-member to only about 6 GPa for the pure Fe end-member.
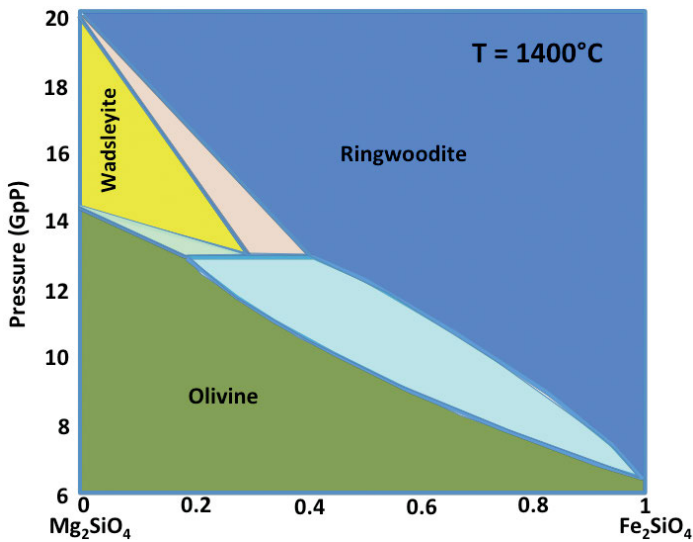

Fig. 5.4: Mg_2SiO_4-Fe_2SiO_4 stability field calculated at 1400 °C as a function of pressure (modified from Frost [6]).

For Mg/Fe compositions typical of the mantle chemistry (i.e. $(Mg_{0.9}Fe_{0.1})_2SiO_4$) at 1400 °C the wadsleyite to ringwoodite transformation was calculated [6] to occur at 17.5 to 18.5 GPa for the Mg-richer composition and at 15 to 16.5 GPa for the Mg-poorer composition. H_2O and Fe^{3+} are predicted to have little effect on the wadsleyite-ringwoodite transformation as they have similar solubility in both wadsleyite and ringwoodite [6].

Thus, ringwoodite and wadsleyite can coexist between 16.5 and 17.5 GPa (about 495 and 525 km depth) at 1285 °C and between about 17.7 and 18.7 GPa (about 531 and 560 km depth) at 1470 °C. The maximum pressure at which ringwoodite can still exist (where wadsleyite is no longer stable) is defined by the ringwoodite breakdown to ferropericlase + bridgmanite, which is widely agreed to occur at an average depth of 660 km with an uncertainty of about 30–50 km (i.e. [5]).

5.5 Thermo-elastic properties of ringwoodite

5.5.1 Bulk modulus

The bulk modulus, defined as $K = -V\partial P/\partial V$, is a key thermodynamic parameter being the inverse of compressibility, which indicates the volume change as a function of pressure. The bulk modulus is a central property that provides information about elasticity of Earth's materials [27]. In order to determine the bulk modulus of ringwoodite we should consider only methods suitable for studying "small samples" in the 0.01–0.1 mm range. Among these techniques, the most widely used are:

(1) in-situ high-pressure X-ray diffraction, which allows under static compression conditions, determination of K_T by studying the unit-cell volume at different pressures and then fitting the pressure-volume data to some equation of state (see [28], EoSFIT7.c).

(2) Brillouin scattering provides the adiabatic bulk modulus K_S and is based on the relationship between the acoustic elastic waves and the elastic moduli and density.

(3) Ultrasonic interferometry is based on wave velocity measurement; the seismic wave velocities Vp and Vs are related to K_S, to the shear modulus G, and to the density of a material.

Finally, in addition to experimental studies there are several computational approaches that should be considered; however, a detailed discussion of these is beyond the scope of this review.

In order to compare the data obtained using the three techniques listed above, an expression relating K_S and K_T is required: $K_S = K_T(1 + \alpha\gamma T)$, with α = thermal expansion, γ = Grüneisen parameter and T = temperature. At low temperature the difference between K_S and K_T is not larger than about 1%, which is of the same magnitude as the experimental uncertainty. However at high temperature such difference becomes significant and the conversion factor $(1 + \alpha\gamma T)$ must be taken into account. For the purpose of a simplified comparison [29] at $T = 298$ the conversion factor is 1.099 for ringwoodite.

Surprisingly, more research has been performed on the effect of water on the bulk modulus of ringwoodite than focusing on the same mineral under dry conditions. This is likely due to the discovery that ringwoodite can host significant amounts of water. In the following paragraph the bulk modulus (and thermal expansion) of dry ringwoodite is analyzed and then the analysis is extended to data from hydrous ringwoodite.

In Tab. 5.3 the values of adiabatic bulk modulus (K_T is converted in K_S by using the conversion factor of 1.099) and its first pressure derivative (where available) are reported for dry ringwoodite. In detail, data for Mg and Fe end-members and intermediate compositions are separated. Analyzing Tab. 5.3 Mg ringwoodite shows general agreement among different studies with an average value of $K_S = 191(11)$ GPa. The

Tab. 5.3: Adiabatic bulk modulus and its first pressure derivative for the ringwoodite-ahrensite solid solution. The data of bulk modulus obtained by X-ray diffraction were converted in adiabatic bulk modulus for purpose of comparison among different techniques.

Composition	K_S	K'	Technique	Reference
Mg_2SiO_4	215	4 (fixed)	X-ray diffraction	[43]
Mg_2SiO_4	184	–	Brillouin	[44]
Mg_2SiO_4	186	4.8 (fixed)	X-ray diffraction	[11]
Mg_2SiO_4	184	4.2	X-ray diffraction	[44]
Mg_2SiO_4	199	4.19	Computational	[45]
Mg_2SiO_4	184	–	Brillouin	[46]
Mg_2SiO_4	185	–	Brillouin	[47]
Mg_2SiO_4	206	4.51	Computational	[48]
Mg_2SiO_4	185	4.5	Ultrasonic	[49]
Mg_2SiO_4	184	4.4	Ultrasonic	[50]
Mg_2SiO_4	185	4.2	Ultrasonic	[51]
$Mg_{1.68}Fe_{0.32}SiO_4$	176	4 (fixed)	X-ray diffraction	[52]
$Mg_{1.84}Fe_{0.16}SiO_4$	188	4.1	Brillouin	[53]
$Mg_{1.8}Fe_{0.2}SiO_4$	192	4.7	X-ray diffraction	[54]
Fe_2SiO_4	209	4.8 (fixed)	X-ray diffraction	[11]
Fe_2SiO_4	220	–	Brillouin	[46]
Fe_2SiO_4	200	4.4	Ultrasonic	[50]
Fe_2SiO_4	203	4.4	Ultrasonic	[51]
Fe_2SiO_4	189	5.5	X-ray diffraction	[13]
Fe_2SiO_4	203	3.7	X-ray diffraction	[55]

first pressure derivative K' on average is 4.35. For intermediate Mg-dominant compositions a similar behavior is observed as for the Mg-end member. For ahrensite (Fe_2SiO_4) a large data scatter with values ranging from 187 to 220 GPa is found. The average value of the adiabatic bulk modulus K_s is 204(10) GPa. The first pressure derivative K' is on average 4.56, in good agreement with the Mg end-member.

Fitting all data in Tab. 5.3 the following linear equation is obtained:

$$K_s \text{ (GPa)} = 203.73 - 0.1447 \times (\% \, Mg_2SiO_4) \tag{5.1}$$

The first pressure derivative K' shows a general agreement with an average value of 4.4(4). The evolution of K_s as a function of Mg_2SiO_4 end-member is displayed in Fig. 5.5.

5.5.2 The effect of water on the bulk modulus of ringwoodite

As ringwoodite can host a considerable amount of structural water in terms of OH groups and this significantly affects its crystal structure, it is quite reasonable to assume that water can also affect the thermodynamic properties.

In Tab. 5.4 all available data on hydrous ringwoodite with Fe up to about 50 % and water content ranging from 0.40 to 2.80 H_2O wt.% are reported. In a first step Fe-free
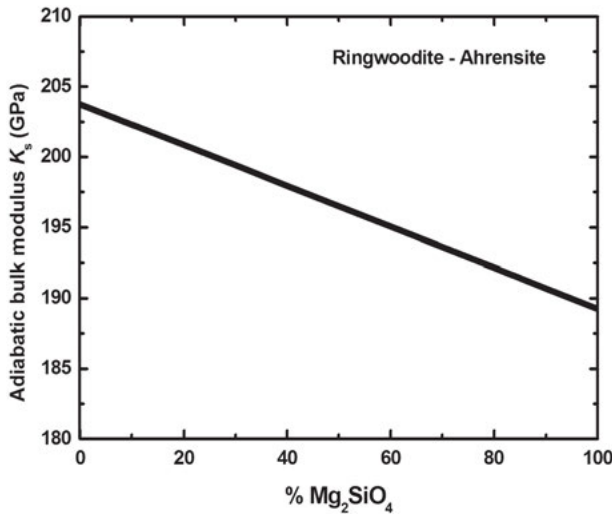
Fig. 5.5: Evolution of the adiabatic bulk modulus, K_s, as a function of the Mg/Fe substitution along the ringwoodite-ahrensite solid solution. The solid line was obtained by using the data in Tab. 5.1 and the relationship (5.1) reported in the text.

ringwoodite with water content between 2.20 and 2.80 % (Tab. 5.2) is considered. The bulk modulus ranges from 165.8 to 149.4 GPa, with an average value of 159(7) GPa and an average K' = 4.9(4).

For Fe-richer samples with 1 % H_2O, the bulk modulus increases to about 176–177 GPa and for samples with 0.4–0.7 % H_2O the bulk modulus reaches the average value of Fe-free anhydrous ringwoodite (Mg_2SiO_4). In order to quantify the effect of water on the bulk modulus for Fe-free ringwoodite the following equation was obtained:

$$K_s \,(\text{GPa}) = 189.8 - 12.607 \times (H_2O \,\text{wt.\% in } Mg_2SiO_4) \tag{5.2}$$

using data in Tab. 5.4 for hydrous ringwoodite and the average bulk modulus of equation (5.1) for a Fe-free ringwoodite. In Fig. 5.6 the variation of K_s for pure Mg_2SiO_4 with the water content is shown.

However, natural ringwoodite is always Fe-bearing requiring knowledge of the effect of H_2O on a Fe-bearing variety. This could be attempted by combining equations (5.1) and (5.2). For equation (5.1) the presence of Fe increases the bulk modulus, whereas for equation (5.2) the presence of water decreases K_s.

Thus, equation (5.3) provides an empirical way of obtaining the adiabatic bulk modulus of ringwoodite as a function of Fe and H_2O content. This equation (5.3) reproduces the data in Tab. 5.4 within an uncertainty of about ±4 GPa if all uncertainties are propagated:

$$K_s \,(\text{GPa}) = [203.73 - 0.1447 \times (\% \, Mg_2SiO_4) - 12.607 \times (H_2O \,\text{wt.\% in } Mg_2SiO_4)] \tag{5.3}$$

Tab. 5.4: Adiabatic bulk modulus and its first pressure derivative for hydrous ringwoodite-ahrensite solid solution. The data of bulk modulus obtained by X-ray diffraction were converted in adiabatic bulk modulus for purpose of comparison among different techniques.

| Composition	Water content	K_S	K'	Technique	Reference
Mg_2SiO_4	2.80 %	149.4	5 (fixed)	X-ray diffraction	[56]
Mg_2SiO_4	2.50 %	161	5.4	X-ray diffraction	[23]
Mg_2SiO_4	2.30 %	165.8	–	Brillouin	[57]
Mg_2SiO_4	2.30 %	166	4.37	Brillouin	[58]
Mg_2SiO_4	2.20 %	155	–	Brillouin	[23]
$Mg_{1.76}Fe_{0.24}SiO_4$	1.00 %	176	4.8 (fixed)	Ultrasound	[59]
$Mg_{1.76}Fe_{0.24}SiO_4$	1.00 %	177	5.3(4)	Ultrasound	[60]
$Mg_{1.76}Fe_{0.24}SiO_4$	1.00 %	177	6.2	X-ray diffraction	[61]
$Mg_{1.78}Fe_{0.22}SiO_4$	0.93 %	169	7.9	X-ray diffraction	[62]
$Mg_{1.90}Fe_{0.10}SiO_4$	0.79 %	176	6.2	X-ray diffraction	[61]
$Mg_{0.98}Fe_{1.02}SiO_4$	0.70 %	188	4 (fixed)	X-ray diffraction	[12]
$Mg_{1.22}Fe_{0.78}SiO_4$	0.40 %	186	4 (fixed)	X-ray diffraction	[12]
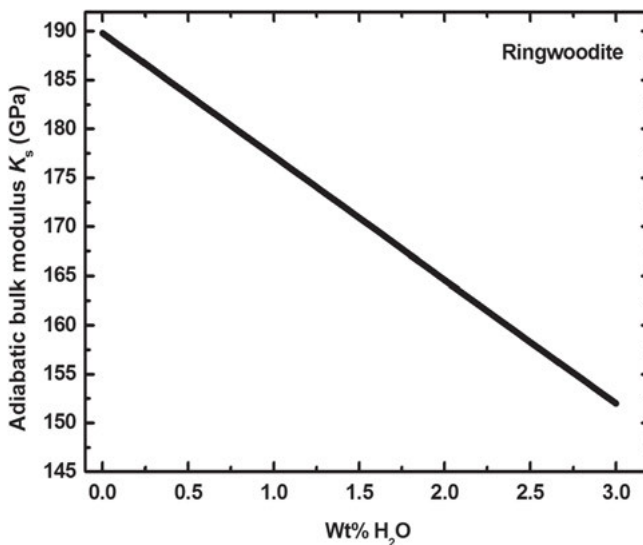
Fig. 5.6: Evolution of the adiabatic bulk modulus, K_s, as a function of the water content in Mg_2SiO_4 ringwoodite. The solid line was obtained by using the data in Tab. 5.2 and the relationship (5.2) reported in the text.

The calculation of (5.3) should not be affected by the first pressure derivative of K_s as the average value for K' for anhydrous ringwoodite is 4.4(4) and 4.9(7) for hydrous ringwoodite. A simple average of these values and their standard deviations ($K' = 4.7(8)$) should yield a reliable result for any ringwoodite composition.

5.5.3 Thermal expansion of anhydrous and hydrous ringwoodite

Thermal expansion, together with compressibility, represents one of the most important thermodynamic parameters. It could be simply defined as the volume variation as a function of temperature at a constant pressure being $\alpha(T) = V^{-1}(\partial V/\partial T)$ (with the only constraint for such expression being $\alpha(T) = (\partial \alpha/\partial T) = 0$ at absolute zero, e.g. [28]). Different thermal expansion equations might be used: the Berman equation, the Fei equation, the Salje equation, the modified Holland and Powell equation or the Kroll form of the Holland and Powell equation as described in detail in [28]. Literature data are applied in this review to determine the volume thermal-expansion coefficient at 298 K, α_{V0} for anhydrous ringwoodite. Only one anhydrous intermediate composition between ringwoodite and ahrensite has been taken into account.

The thermal expansion data for "dry" and hydrous ringwoodite are reported in Tab. 5.5. The data for anhydrous Mg_2SiO_4 show in general significant scatter but the average value is $\alpha_{V0} = 2.3(5) \times 10^{-5}$ K^{-1}. The intermediate composition, $(Mg_{0.91}Fe_{0.09})_2SiO_4$, shows a similar volume thermal-expansion and also anhydrous Fe_2SiO_4 has an average value of $\alpha_{V0} = 2.3(2) \times 10^{-5}$ K^{-1}. Apparently, there is no change in thermal expansion along the ringwoodite-ahrensite solid-solution series.

Tab. 5.5: Volume thermal expansion data for anhydrous and hydrous ringwoodite-ahrensite solid solution.

Composition	Water content	α_{V0} (×10^{-6}/K)	Technique	Reference
Mg_2SiO_4	0	1.90	X-ray diffraction	[63]
Mg_2SiO_4	0	2.37	Calorimetry	[64]
Mg_2SiO_4	0	1.77	X-ray diffraction	[47]
Mg_2SiO_4	0	2.70	HPVS*	[65]
Mg_2SiO_4	0	3.07	X-ray diffraction	[24]
Mg_2SiO_4	0	2.57	X-ray diffraction	[66]
Mg_2SiO_4	0	1.97	Computational	[67]
Mg_2SiO_4	0	2.74	Computational	[68]
Mg_2SiO_4	0	1.75	Computational	[69]
$Mg_{1.82}Fe_{0.18}SiO_4$	0	2.50	X-ray diffraction	[70]
Fe_2SiO_4	0	2.30	X-ray diffraction	[71]
Fe_2SiO_4	0	2.46	Thermochemical	[72]
Fe_2SiO_4	0	2.62	X-ray diffraction	[73]
Fe_2SiO_4	0	2.15	Computational	[74]
Fe_2SiO_4	0	2.13	Computational	[75]
Mg_2SiO_4	2.60 %	2.73	X-ray diffraction	[23]
Mg_2SiO_4	2.50 %	2.90	X-ray diffraction	[24]

*High-pressure vibrational spectroscopy

Few results [30] are not covered by Tab. 5.5. The excluded data were affected by "disequilibrium irreversible expansion starting already at 606 K" [30]. For water contents between 2.50 and 2.60 wt.% H_2O the average thermal expansion coefficient is $\alpha_{V0} = 2.8(1) \times 10^{-5}\,K^{-1}$. Although only two data sets are used for the present comparison, it seems that water increases the thermal expansion of ringwoodite by about 17–18 %. Combining the data in Tab. 5.5 the following equation is derived:

$$\alpha_{V0} = 2.316 \times 10^{-5}\,K^{-1} + 0.195 \times (\text{wt.\% } H_2O \text{ in } Mg_2SiO_4). \qquad (5.4)$$

Equation (5.4) thus takes into account the effect of Fe and water on the thermal expansion coefficient of ringwoodite.

5.5.4 Thermo-elastic properties of ringwoodite: implications for Earth Sciences

How could the change of the bulk modulus and of the thermal expansion as a function of composition and water content be used in Earth Sciences obtaining geophysical information? It was recently demonstrated that the new approach of so-called "elastic geobarometry" can be applied to any mineral inclusion entrapped in a mineral host. Such an approach, developed by Angel et al. [31], is mainly based on the difference of thermo-elastic properties between host and inclusion and on the residual pressure to which the inclusion is still exposed when the host is at atmospheric pressure. A very good example is represented by diamond and its mineral inclusions. Due to the very high bulk modulus and very low thermal expansion coefficient, diamond shows a much smaller expansion when it reaches the surface from the mantle. In contrast, the inclusions in diamond tend to expand much more as their thermo-elastic properties are strongly different from those of diamond. In general, diamond has at least a 2–3 times larger bulk modulus than common silicates found in it as inclusions and a thermal expansion, which is at least 3 times smaller [31]. This means that, for those diamond-inclusion pairs not showing any cracks at atmospheric pressure, the inclusion is always under some pressure (i.e. 0.4–0.5 GPa, see [15]), which is called "residual or remnant or internal pressure".

If such a geobarometric method is applied to the diamond-ringwoodite pair important information on the possible depth of entrapment can be obtained. The software EosFit7c [28] was used to perform the calculation of the elastic properties for a pure Mg anhydrous ringwoodite, a Fe-rich ringwoodite, and a very hydrous ringwoodite like the one found in the Brazilian diamond by Pearson et al. [32].

A ringwoodite host within diamond, not surrounded by cracks, is assumed to have a possible internal pressure of 5 GPa. For a temperature of 2000 °C in the transition zone, a pressure of formation (or entrapment) for the diamond-ringwoodite pair can be calculated that is equal to 22.7 GPa for a pure anhydrous Mg ringwoodite. Adding some Fe (20 %) to the anhydrous ringwoodite such calculation provides a pressure of 22.9 GPa, so the difference is not significant as the bulk modulus and the thermal ex-

pansion as a function of the Mg/Fe substitution do not show large variations (at least for limited substitutions). If instead, the same calculation is performed for a hydrous ringwoodite, with a water concentration (ca. 1.4 wt.%) similar to the one found in a diamond inclusion [32], then at 2000 °C the pressure of formation is reduced to 17.2 GPa. These results are of high importance because it is known that the pressure of formation obtained above for anhydrous ringwoodite (regardless the Fe content at least up to 20 % in molar fraction of Fe_2SiO_4) are too high and fall in the ferropericlase + bridgmanite stability field. In contrast, the pressure of formation obtained for hydrous ringwoodite leads to the transition zone at about 515–516 km depth, which nearly overlaps with the wadsleyite – ringwoodite phase boundary. Thus, this is proof that the presence of water decreases the pressure of the ringwoodite stability field. However, the true values are strongly dependent on the quality of the thermo-elastic parameters. To conclude, we hope that in future it will be possible to measure the unit-cell parameters and the crystal structure of a natural ringwoodite still trapped in a diamond in order to obtain reliable geobarometric data.

5.6 Ascent of diamond-bearing kimberlite magma

The discovery of ringwoodite in diamond not only provided a new scenario relatively to the real amount of water stored in Earth but at the same time it could provide new constraints on the debate about the ascent velocity of diamond-bearing kimberlite magmas. This topic has been strongly discussed in the literature and still doubts remain. The literature data suggest an ascent velocity from some meters per second to tens of meters per second [33].

One of the most recent contributions to this issue originates from Baruah et al. [34]. These authors tackled the "rapid ascent problem" by a multi-directional approach: they took into account (a) the kinetics of the diamond-graphite transformation, (b) the settling velocity of diamond phenocrysts in magmas, (c) the formation of ruptures during high-speed magma ascent. Such an approach is reasonable, as none of the above points must be neglected to provide a reliable value of ascent velocity.

In detail, Baruah et al. [34] measured the degree of graphitization of diamond as a function of the ascent velocity in a synthetic kimberlitic diamond-bearing magma (also varying the starting compositions). Even if the authors cannot provide a "single number" for their final results they propose an ascent velocity higher than 10 m/s. It must be remarked that even for this ascent velocity they find some degree of graphitization on very small diamonds. Unfortunately, the authors [34] did not provide measurements for velocities higher than 10 m/s. Averaging their measured data, a reasonable velocity for large diamond with no evidence of graphitization can be estimated to be around 20 m/s (or about 72 km/h). Octahedral lithospheric diamond, up to several mm large, with no traces of graphitization is quite common (see [35]). For such dia-

monds the ascent time may be estimated to last a couple of hours assuming a possible depth of formation at around 150 km [15].

If for "super-deep" diamonds similar ascent velocities are assumed, such diamond travels from the transition zone, about 550 km, to the surface in less than 8 hours. It is known from ringwoodite found in a Brazilian diamond that its host diamond crystallized at least at a depth of 525 km. However, it remains unknown whether the diamond reached the Earth's surface in one single "trip" from 525 km or this long journey had multiple stages, characterized by a first very fast ascent reaching some depths under the cratonic area at which the temperature was too low to allow back-transformation of ringwoodite to olivine. Unfortunately, there are no kinetic data that could reveal how fast the back-transformation of ringwoodite to olivine is, and at the same time it needs to be considered that such a transformation should occur inside diamond. Thus, for a meaningful study of such kinetic processes it will be necessary to obtain large diamond crystals containing ringwoodite and at present such experiments appears to be highly unlikely.

5.7 Ringwoodite and the Earth's storage water capacity

The Earth's water storage capacity is one of the most debated scientific issues in Earth Sciences. For decades scientist have been trying to find out how much water is stored in our planet. Several investigations addressed this topic and one of the recent reviews [36] indicates a total mass of water equal to 3.04×10^{24} g. An even more recent review [37] recalculates the mass of water at 5.50×10^{24} g. This difference is primarily due to the crucial discovery [32] of a crystal of hydrous ringwoodite enclosed within a "super-deep" diamond from Brazil characterized by a water concentration of about 1.4 wt.% (Fig. 5.7). A recent study [38] confirmed this water concentration by using a new IR calibration and reported a concentration of 1.43(27) wt.% H_2O for the ringwoodite inclusion [32]. This water concentration represents about 50 % of the maximum water solubility in ringwoodite and is different from previous assumptions about natural ringwoodite compositions. Furthermore, if ringwoodite is hydrous there are no reasons to think that wadsleyite is not. Even if these two minerals in the transition zone could host half of their maximum water solubility, as found in laboratory, such a finding could change the complete scenario of the water cycle on our planet. This discovery would also explain why, compared to the amount water determined for CI carbonaceous chondritic meteorites, which is about 10 % ([39] and references therein), the Earth appeared so dry. Apparently the difference between the water content on the Earth and that in CI chondrites is much smaller than that previously estimated and this could be due to ringwoodite and wadsleyite in the transition zone.

Some authors actually suggested that ringwoodite found in diamond may only represent a locally water-rich enrichment and be unrepresentative of the real water concentration of the transition zone (e.g. [40]). Although this explanation cannot be
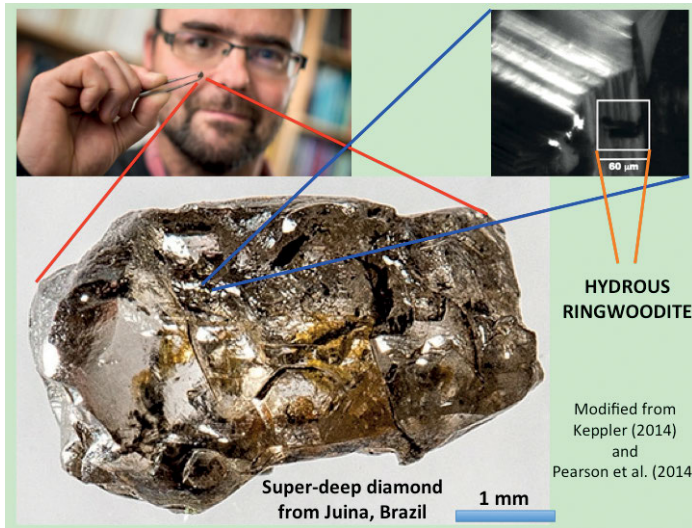
Fig. 5.7: Dr. Graham Pearson (top left) holding the diamond from Juina in which for the first time hydrous ringwoodite was found in the Earth [32]. On bottom left a magnification of the diamond and on top right a magnification of the tiny hydrous ringwoodite grain. The images are modified from [32] and [40]. The picture of the diamond is from Richard Siemens (University of Alberta).

ruled out, a recent study on the transformation of hydrous ringwoodite to $MgSiO_3$ bridgmanite plus (Mg,Fe)O (occurring at 660 km depth) documented the formation of intergranular melt and this might be consistent with large hydrated regions in the transition zone [41]. Moreover, a strongly hydrated transition zone has been proposed by geophysicists (i.e. [42]) and although the level of hydration of the transition zone has not been proven conclusively, thanks to ringwoodite any future geophysical model of this region and of the entire Earth must take into account much more water than previously thought.

Bibliography

[1]   Spencer LJ. The Tenham (Queensland) meteoritic shower of 1879. Mineral Mag 1937, 24, 437–457.

[2]   Binns RA, Davis RJ, Reed SJB. Ringwoodite, natural $(Mg,Fe)_2 SiO_4$ spinel in the Tenham meteorite. Nature 1969, 221, 943–944.

[3]   Chen M, El Goresy A, Gillet P. Ringwoodite lamellae in olivine: clues to olivine-ringwoodite phase transition mechanisms in shocked meteorites and subducting slabs. Proc Natl Acad Sci USA 2004, 42, 15033–15037.

[4]   Ringwood AE, Major A. High pressure transformations of spinels (I). Earth Planet Sci Lett 1966, 5, 242–250.

[5]   Frost DJ. The upper mantle transition zone. Elements 2008, 4, 171–176.

[6]   Frost DJ. The structure and sharpness of $(Mg,Fe)_2 SiO_4$ phase transformations in the transition zone. Earth Planet Sci Lett 2003, 216, 313–328.

[7]   Agee CB. Phase transformations and seismic structure in the upper mantle and transition zone. In: Hemley RJ (ed) Ultrahigh-Pressure Mineralogy. Rev Mineral Geochem 1998, 37, 165–203.

[8]   Dziewonski AM, Anderson DL. Preliminary reference Earth model. Phys Earth Planet Inter 1981, 25, 297–356.

[9]   Kohlstedt DL, Keppler H, Rubie DC. Solubility of water in the α, β, and γ phases of $(Mg,Fe)_2 SiO_4$. Contrib Mineral Petrol 1996, 123, 345–357.

[10]   Ma C, Tschauner O, Liu Y, Sinogeikin S. Ahrensite, IMA 2013-028. CNMNC Newsletter No. 16, August 2013, page 2707; Mineral Mag 2013, 77, 2695–2709.

[11]   Hazen RM, Downs RT, Finger LW, Ko J. Crystal chemistry of ferromagnesian silicate spinels: evidence for Mg-Si disorder. Am Mineral 1993, 78, 1320–1323.

[12]   Ganskow G, Boffa Ballaran T, Langenhorst F. Effect of iron on the compressibility of hydrous ringwoodite. Am Mineral 2010, 95, 747–753.

[13]   Nestola F, Boffa Ballaran T, Koch-Mueller M, Balic-Zunic T, Taran M, Olsen L, Princivalle F, Secco L, Lundegaard L. New accurate compression data for γ-$Fe_2 SiO_4$. Phys Earth Planet Inter 2010, 183, 421–425.

[14]   Kamb B. Structural basis of the olivine-spinel stability relation. Am Mineral 1968, 53, 1439–1455.

[15]   Nestola F, Nimis P, Ziberna L, Longo M, Marzoli A, Harris JW, Manghnani MH, Fedortchouk Y. First crystal-structure determination of olivine in diamond: composition and implications for provenance in the Earth's mantle. Earth Planet Sci Lett 2011, 305, 249–255.

[16]   Holl CM, Smyth JR, Jacobsen SD, Frost DJ. Effects of hydration on the structure and compressibility of wadsleyite β-$(Mg_2 SiO_4)$. Am Mineral 2008, 93, 598–607.

[17]   Nestola F, Balic-Zunic T, Koch-Mueller M, Secco L, Princivalle F, Parisi F, Dal Negro A. High-pressure crystal structure investigation of synthetic $Fe_2 SiO_4$ spinel. Mineral Mag 2011, 75, 2649–2655.

[18]   Nakatsura A, Yoshiasa A, Yamanaka T, Ohtaka O, Katsura T, Ito E. Symmetry change of majorite solid-solution in the system $Mg_3 Al_2 Si_3 O_{12}$ – $MgSiO_3$. Am Mineral 1999, 82, 1135–1143.

[19]   Collerson KD, Hapugoda S, Kamber BS, Williams Q. Rocks from the mantle transition zone: majorite-bearing xenoliths from Malaita, Southwest Pacific. Science 2000, 288, 1215–1223.

[20]   Yamanaka T, Fukuda T, Tsuchiya J. Bonding character of SiO_2 stishovite under high pressures up to 30 GPa. Phys Chem Miner 2002, 29, 633–641.

[21]   Gasparik T. The role of volatiles in the translation zone. J Geophys Res 1993, 98, 4287–4299.

[22]   Smyth JR. β-$Mg_2 SiO_4$; a potential host for water in the mantle? Am Mineral 1987, 72, 1051–1055.

[23] Inoue T. Effects of water on melting phase relations and melt composition in the system Mg_2SiO_4-$MgSiO_3$-H_2O to 15 GPa. Phys Earth Planet Inter 1994, 85, 237–263.

[24] Ye Y, Brown DA, Smyth JR, Panero WR, Jacobsen SD, Chang YY, Townsend JP, Thomas SM, Hauri EH, Dera P, Frost DJ. Compressibility and thermal expansion of hydrous ringwoodite with 2.5(3) wt.% H_2O. Am Mineral 2012, 97, 573–582.

[25] Smyth J, Holl CM, Frost DJ, Jacobsen SD, Langenhorst F, McCammon C. Structural systematics of hydrous ringwoodite and water in Earth's interior. Am Mineral 2003, 88, 1402–1407.

[26] Panero WR, Smyth JR, Pigott JS, Liu Z, Frost DJ. Hydrous ringwoodite to 5 K and 35 GPa: Multiple hydrogen bonding sites resolved with FTIR spectroscopy. Am Mineral 2013, 98, 637–642.

[27] Angel RJ, Jackson JM, Reichmann HJ, Speziale S. Elasticity measurements on minerals: a review. Eur J Mineral 2009, 21, 525–550.

[28] Angel RJ, Gonzalez-Platas J, Alvaro M. EosFit7c and a Fortran module (library) for equation of state calculations. Z Kristallogr 2014, 229, 405–419.

[29] Li L, Weidner DJ, Brodholt J, Alfe D, Price GD. Elasticity of Mg_2SiO_4 ringwoodite at mantle conditions. Phys Earth Planet Inter 2006, 157, 181–187.

[30] Ye Y, Schwering RA, Smyth JR. Effects of hydration on thermal expansion of forsterite, wadsleyite, and ringwoodite at ambient pressure. Am Mineral 2009, 94, 899–904.

[31] Angel RJ, Alvaro M, Nestola F, Mazzucchelli ML. Diamond thermoelastic properties and implications for determining the pressure of formation of diamond-inclusion systems. Russ Geol Geophys 2015, 56, 211–220.

[32] Pearson DG, Brenker FE, Nestola F, McNeill J., Nasdala L, Hutchison MT, Matveev S, Mather K, Silversmit G, Schmitz S, Vekemans B, Vincze L. Hydrous mantle transition zone indicated by ringwoodite included within diamond. Nature 2014, 507, 221–224.

[33] Sparks RSJ, Baker L, Brown RJ, Field M, Schumacher J, Stripp G, Walters A. Dynamical constraints on kimberlite volcanism. J Volcanol Geotherm Res 2006, 15, 18–48.

[34] Baruah A, Gupta AK, Mandal N, Singh RN. Rapid ascent conditions of diamond-bearing kimberlitic magmas: Findings from high pressure–temperature experiments and finite element modeling. Tectonophysics 2013, 594, 13–26.

[35] Nestola F, Nimis P, Angel RJ, Milani S, Bruno M, Prencipe M, Harris JW. Olivine with diamond-imposed morphology included in diamonds. Syngenesis or protogenesis? Int Geol Rev 2014, 56, 1658–1667.

[36] Bodnar RJ, Azbej T, Becker SP, Cannatelli C, Fall A, Severs MJ. Whole Earth geohydrologic cycle, from the clouds to the core: The distribution of water in the dynamic Earth system, *in* Bickford, M.E., ed., The Web of Geological Sciences: Advances, Impacts, and Interactions: Spec Pap – Geol Soc Am 2013, 500, 431–461.

[37] Nestola F, Smyth JR. Diamonds and water in the deep Earth: a new scenario. Int Geol Rev 2015, in press. DOI: 10.1080/00206814.2015.1056758.

[38] Thomas SM, Jacobsen SD, Bina CR, Reichart P, Moser M, Hauri EH, Koch-Müller M, Smyth, JR, Dollinger G. Quantification of water in hydrous ringwoodite. Front Earth Sci 2015, doi: 10.3389/feart.2014.00038.

[39] Kerridge F. Carbon, hydrogen and nitrogen in carbonaceous chondrites: abundances and isotopic compositions in bulk samples. Geochim Cosmochim Acta 1985, 49, 1707–1714.

[40] Keppler H. Earth's deep water reservoir. Nature 2014, 507, 174–175.

[41] Schmandt B, Jacobsen SD, Becker TW, Zhenxian L, Dueker KG. Dehydration melting at the top of lower mantle. Science 2014, 344, 1265–1268.

[42] Bercovici D, Karato S. Whole-mantle convection and the transition-zone water filter. Nature 2003, 425, 39–44.

[43] Mizukami S, Ohtani A, Kawai N. High-pressure X-ray diffraction studies on β- and γ-Mg2SiO4. Phys Earth Planet Inter 1975, 10, 177–182.

[44] Meng Y, Weidner DJ, Gwanmesia GD, Liebermann RC, Vaughan MT, Wang Y, Leinenweber K, Pacalo RE, Yeganeh-Haeri A, Zhao Y. In Situ high P-T X-ray diffraction studies on three polymorphs (α, β, γ) of Mg_2SiO_4. J Geophys Res 1993, 98, 22199–22207.

[45] Kiefer B, Stixrude L, Wentzcovitch RM. Calculated elastic constants and anisotropy of Mg_2SiO_4 spinel at high pressure. Geophys Res Lett 1997, 24, 2841–2844.

[46] Sinogeikin SV, Katsura T, Bass JD. Sound velocities and elastic properties of Fe-bearing wadsleyite and ringwoodite. J Geophys Res 1998, 103, 20819–20825.

[47] Jackson JM, Sinogeikin SV, Bass JD. Sound velocities and elastic properties of γ-Mg_2SiO_4 to 873 K by Brillouin spectroscopy. Am Mineral 2000, 85, 296–303.

[48] Bukowinski MST, Downs JW. Structures, compressibilities and relative stabilities of the alpha, beta and gamma phases of Mg_2SiO_4 deduced from an electron-gas ionic Hamiltonian. Geophys J Int 2000, 143, 295–301.

[49] Li B. Compressional and shear wave velocities of ringwoodite γ-Mg_2SiO_4 to 12 GPa. Am Mineral 2003, 88, 1312–1317.

[50] Higo Y, Inoue T, Li BS, Irifune T, Liebermann RC. The effect of iron on the elastic properties of ringwoodite at high pressure. Phys Earth Planet Inter 2006, 159, 276–285.

[51] Liu Q, Liu W, Whitaker ML, Wang L, Li B. Compressional and shear wave velocities of Fe_2SiO_4 spinel at high pressure and high temperature. High Pressure Res 2008, 28, 405–413.

[52] Fei YW, Mao HK, Shu JF, Parthasarathy G, Bassett WA, Ko JD. Simultaneous high-P, high-T X-ray-diffraction study of beta-$(Mg,Fe)_2SiO_4$ to 26-GPa and 900-K. J Geophys Res 1992, 97, 4489–4495.

[53] Sinogeikin SV, Bass JD, Katsura T. Single-crystal elasticity of ringwoodite to high pressures and high temperatures: Implications for 520 km seismic discontinuity. Phys Earth Planet Inter 2003, 136, 41–66.

[54] Matsui M, Katsura T, Kuwata A, Hagiya K, Tomioka N, Sugita M, Yokoshi S, Nozawa A, Funakoshi K. Equation of state of $(Mg_{0.8}Fe_{0.2})_2SiO_4$ ringwoodite from synchrotron X-ray diffraction up to 20 GPa and 1700 K. Eur J Mineral 2006, 18, 523–528.

[55] Greenberg E, Dubrovinsky LS, McCammon C, Rouquette J, Kantor I, Prakapenka V, Rozenberg GK, Pasternak MP. Pressure-induced structural phase transition of the iron end-member of ringwoodite (gamma-Fe_2SiO_4) investigated by X-ray diffraction and Mossbauer spectroscopy. Am Mineral 2011, 96, 833–840.

[56] Yusa H, Inoue T, Ohishi Y. Isothermal compressibility of hydrous ringwoodite and its relation to the mantle discontinuities. Geophys Res Lett 2000, 27, 413–416.

[57] Wang J, Sinogeikin SV, Inoue T, Bass JD. Elastic properties of hydrous ringwoodite. Am Mineral 2003, 88, 1608–1611.

[58] Wang J. Elastic properties of hydrous ringwoodite at high-pressure conditions. Geophys Res Lett 2006, 33, L14308.

[59] Jacobsen SD, Smyth JR, Spetzler H, Holl CM, Frost DJ. Sound velocities and elastic constants of iron-bearing hydrous ringwoodite. Phys Earth Planet Inter 2004, 143, 47–56.

[60] Jacobsen SD, Smyth JR. Effect of water on the sound velocities of ringwoodite in the transition zone. In S.D. Jacobsen and S. Van der Lee, Eds., Earth's Deep Water Cycle 2006, 168, p. 131–145. Am Geophys Union, Geophys Monogr, Washington, D.C.

[61] Manghnani MH, Amulele G, Smyth JR, Holl CM, Shen G, Prakapenka V. Equation of state of hydrous Fo90 ringwoodite to 45 GPa by synchrotron powder diffraction. Mineral Mag 2005, 69, 317–324.

[62] Smyth JR, Holl CM, Frost DJ, Jacobsen SD. High pressure crystal chemistry of hydrous ringwoodite and water in the Earth's interior. Phys Earth Planet Inter 2004, 143, 271–278.

[63] Suzuki I, Ohtani Em Kumazawa M. Thermal expansion of γ-Mg_2SiO_4. J Phys Earth 1979, 27, 53–61.

[64] Akaogi M, Ito E, Navrotsky A. Olivine-modified spinel-spinel transitions in the system Mg_2SiO_4-Fe_2SiO_4 – calorimetric measurements, thermochemical calculation, and geophysical application. J Geophys Res 1989, 94, 15671–15685.

[65] Chopelas A. Thermal expansivity of mantle relevant magnesium silicates derived from vibrational. spectroscopy at high pressure. Am Mineral 2000, 85, 270–278.

[66] Katsura T, Yokoshi S, Song M, Kawabe K, Tsujimura T, Kubo A, Ito E, Tange Y, Tomioka N, Saito K, Nozawa A, Funakoshi K. Thermal expansion of Mg_2SiO_4 ringwoodite at high pressures. J Geophys Res 2004, 109, B12209.

[67] Yu YG, Wentzcovitch RM. Density functional study of vibrational and thermodynamic properties of ringwoodite. J Geophys Res 2006, 111, B12202.

[68] Li L, Weidner DJ, Brodholt J, Alfe D, Price GD. Elasticity of Mg_2SiO_4 ringwoodite at mantle conditions. Phys Earth Planet Inter 2006, 157, 181–187.

[69] Ottonello G, Civalleri B, Ganguly J, Zuccolini Vetuschi M, Noel Y. Thermophysical properties of the alpha-beta-gamma polymorphs of Mg_2SiO_4: a computational study. Phys Chem Miner 2009, 36, 87–106.

[70] Nishihara Y, Takahashi E, Matsukage KN, Iguchi T, Nakayama K, Funakoshi K. Thermal equation of state of $(Mg_{0.91}Fe_{0.09})_2SiO_4$ ringwoodite. Phys Earth Planet Inter 2004, 143, 33–46,

[71] Yagi T, Akaogi M, Shimomura O, Suzuki T, Akimoto S. In situ observation of the olivine-spinel phase-transformation in Fe_2SiO_4 using synchrotron radiation. J Geophys Res 1987, 92, 6207–6213.

[72] Fei YW, Saxena SK. A thermochemical database for phase-equilibria in the system Fe-Mg-Si-O at high-pressure and temperature. Phys Chem Miner 1986, 13, 311–324.

[73] Plymate TG, Stout JH. Pressure-volume-temperature behavior of gamma-Fe_2SiO_4 (spinel) based on static compression measurements at 400 ºC. Phys Chem Miner 1994, 21, 413–420.

[74] Yu YG, Vinograd VL, Winkler B, Wentzcovitch RM. Phase equilibria of $(Mg,Fe)_2SiO_4$ at the Earth's upper mantle conditions from first-principles studies. Phys Earth Planet Inter 2013, 217, 36–47.

[75] Jacobs MHG, de Jong BHWS. An investigation into thermodynamic consistency of data for the olivine, wadsleyite and ringwoodite form of $(Mg,Fe)_2SiO_4$. Geochimica et Cosmochimica Acta 2005, 69, 4361–4375.